für Hochfrequenztechnik (Electrical Engineering Department of the Technical University Braunschweig), where he has been involved with investigations on high-speed modulators for PCM communication systems and on amplification and noise in solid-state oscillators. He is now a Professor in the Electrical Engineering Department and his current research interests are primarily concerned with new technologies for microwave integrated circuits, such as fin-line and waveguide-below-cutoff techniques, and with transport phenomena in submicron structures.

Modal Solutions of Active Dielectric Waveguides by Approximate Methods

A. LINZ, MEMBER, IEEE, AND J. K. BUTLER, SENIOR MEMBER

Abstract—**Approximate methods are used to obtain the modal properties of stripe-contact semiconductor injection lasers using a planar three-layer waveguide model. The central active layer has a dielectric constant that varies smoothly along the direction parallel to the heterojunction boundaries. The complex dielectric constant under the stripe contact is dependent on the gain and approaches a constant value at large lateral distances. The two methods are compared in terms of their modal propagation constants. An application of the effective index method facilitates a physical understanding of dielectric waveguide modes as well as providing an efficient calculation procedure.**

I. INTRODUCTION

ANALYSIS OF mode propagation in dielectric waveguides with a spatially varying refractive index has been the subject of several papers [1]–[3]. Typically, the variation of the dielectric constant with distance has been approximated with a parabolic profile [1], [2] or a function of the form $\kappa = -\kappa_0 + \kappa_3 \tanh^2(x/x_0)$ [3]. Both approximations have the disadvantage that the value of κ goes to infinity at large distances from the point $x = 0$, which corresponds to the axis of lateral symmetry of the structure. In the case of a semiconductor laser, this corresponds to the region below the center of the contact stripe. Another approximation that eliminates this disadvantage is the use of a function of the form [4]

$$\kappa = \kappa_S + \Delta\kappa/\cosh^2(x/x_0) \tag{1}$$

to describe the variation of κ. This is in closer correspondence with the physical situation, since κ now acquires the value κ_S for $x \gg x_0$. Even if this particular form of variation of κ does not describe the actual variation very closely, it retains the most important features, and leads to equations with known solutions. The disadvantage in this case is the fact that the field solutions consist of a finite (possibly empty) set of confined trapped modes, an infinite set of discrete, diverging "leaky" modes, and a continuum of solutions that will be designated as "radiation" modes, as opposed to an infinite set of discrete trapped modes only, as in the parabolic and $\tanh^2(x/x_0)$ profiles. Mode analysis is a two-dimensional problem, since the refractive index varies in both lateral (x) and transverse (y) directions. Therefore, numerical or approximate methods need to be applied. The most popular and effective approximation method is the "effective-index" solution, whereby the two-dimensional problem is reduced to an equivalent, one-dimensional one [2], [4]–[8]. Numerical methods have also been developed. For example, in [1] the parabolic variation is used. Maxwell's equations are solved both for the active layer and the confining layers, and then superposition is applied to both types of solutions to form a general expression for the field. These solutions and their derivatives are matched at the boundaries of the active layer, yielding an infinite system of linear homogeneous equations, whose solutions, numerically obtained, are the expansion coefficients for the mode in terms of the eigenfunctions of the active layer problem. Of course, direct numerical integration of the two-dimensional wave equation is possible, but the computation times are long compared to those required by the algorithm discussed in this paper.

For the type of variation considered here, a general field in the active layer must be expressed as a superposition of the few confined discrete modes plus an integral over the continuum. Leaky modes cannot be included in the expansion if the field is to decrease to zero for large distances from the stripe.

Direct application of the numerical method used in [1] results in a finite set of linear equations (due to the finite number of trapped modes) coupled with an integral equation (due to integral over the continuum). For the case in which only one trapped mode exists (the fundamental mode), an integral equation results, which can in principle be solved. However, these cases will be seen to correspond to structures with net modal loss or low gains very sensitive

Manuscript received May 6, 1982; revised June 22, 1982. This work was supported by the U.S. Army Research Office.

The authors are with the Department of Electrical Engineering, Southern Methodist University, Dallas, TX 75275.

0018-9480/82/1200-2139$00.75 ©1982 IEEE

to the dielectric step size. For structures that exhibit higher, stable gain, several discrete trapped modes exist, and we achieve reasonable convergence with the first few modes, so that considering the continuum is not necessary. We also apply the effective-index method and compare it with the approximate numerical method in terms of the propagation constant γ, which is calculated as a function of the dielectric step size in the active layer $\Delta n = n_0 - n_S$, where n_0 and n_S are the values of refractive index under the stripe and far away from it. The results of the two methods practically coincide for the cases in which several trapped modes exist. They differ appreciably only for that range of Δn for which only one trapped mode exists. The discrepancy may be possibly due to the continuum, but this paper does not investigate this matter further. The following sections will consist of a description of the class of waveguides considered, followed by a description of the approximate numerical method, ending with the application of the effective-index method to this problem and conclusions.

II. Description of Structures

Fig. 1 shows the structure considered in this paper. The confining layers A and C are assumed identical, their refractive indices being described by

$$\kappa_A = \kappa_C \cong n_A^2 - i\alpha_A n_A / k_0. \tag{2}$$

α_A describes the power loss in these layers, and is constant with distance. The active layer has a constant thickness d, with a refractive index

$$\kappa(x) = n^2(x) - i\alpha(x)n(x)/k_0 \tag{3}$$

whose dependence with x is considered to be reasonably well approximated by

$$\kappa(x) = \kappa_S + \Delta\kappa/\cosh^2(x/x_0) \tag{4}$$

where

$$\Delta\kappa = \kappa_0 - \kappa_S \tag{5a}$$

$$\kappa_0 = \kappa(0) = n_0^2 + ig_0 n_0/k_0 \tag{5b}$$

$$\kappa_S = n_S^2 - i\alpha_S n_S/k_0. \tag{5c}$$

x_0 is a parameter related to the width of the stripe. The values of power attenuation coefficient and refractive index inside the active region far away from the stripe are α_S and n_S, respectively. The quantity g_0 represents power gain under the stripe, where the refractive index is n_0, and $k_0 = 2\pi/\lambda$.

Using (4) and (5), we can obtain expressions for the variation of the refractive index n and the loss α (or gain $-\alpha$) as a function of distance. Figs. 2 and 3 show $n(x)$ versus x/x_0 and $\alpha(x)$ versus x/x_0. For $\Delta n = n_0 - n_S > 0$, the mode will be index-guided, while for $\Delta n < 0$, it will be index-antiguided. In this latter case, it will still be confined because of the gain distribution, but the field will be more spread and the modal gain will be low (eventually we may have a net power loss). If Δn is negative enough, the guiding effect is lost and the modes become leaky. The condition $\Delta n > 0$ results in strong confinement and high and stable values of modal gain.

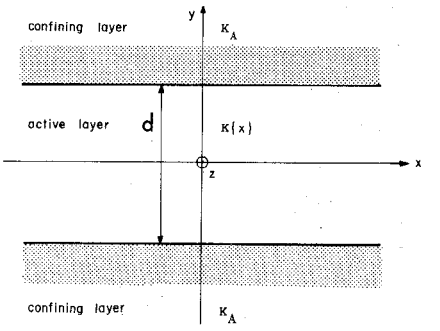

Fig. 1. Waveguide structure considered.

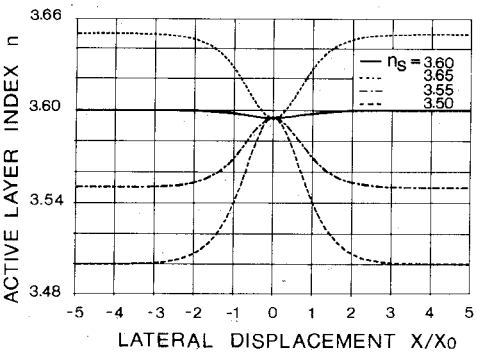

Fig. 2. Refractive index of active layer versus lateral displacement for $\alpha_S = 50\ \text{cm}^{-1}$, $g_0 = 200\ \text{cm}^{-1}$, $n_0 = 3.595$ for different values of n_S.

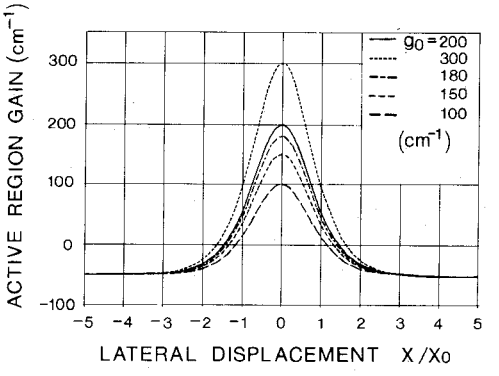

Fig. 3. Power gain $-\alpha$ for active region versus lateral displacement for $\alpha_S = 50\ \text{cm}^{-1}$, $n_0 = 3.595$, $n_S = 3.6$ for different values of g_0.

III. Numerical Solution

We assume an electric field of the form

$$E_x = \Psi(x, y). \tag{6}$$

Following [1], we apply Maxwell's equations to the structure in Fig. 1, and obtain inside the active layer

$$\nabla_t^2 \Psi_b + \left[\gamma^2 + k_0^2 \kappa(x)\right]\Psi_b = 0 \tag{7}$$

and outside the active layer

$$\nabla_t^2 \Psi_a + \left[\gamma^2 + k_0^2 \kappa_A\right]\Psi_a = 0 \tag{8}$$

where $\kappa(x)$ is given by (4). We require the functions Ψ_a and Ψ_b and their normal derivatives to be continuous at the

boundaries $y = \pm d/2$, and demand that Ψ_a and Ψ_b decrease to zero as $x \to \pm\infty$, and also that $\Psi_a \to 0$ as $|y| \to \infty$. These boundary conditions are homogeneous, so we can apply separation of variables.

First we consider the solution inside the active layer making

$$\Psi_b(x, y) = \psi(x)\phi(y). \tag{9}$$

Substitution in (7) results in a vertical solution of the form

$$\phi(y) = \begin{pmatrix} \sin \\ \cos \end{pmatrix} qy \tag{10a}$$

and a differential equation

$$\frac{d^2\psi}{dx^2} + \left[k_0^2\kappa_S + \gamma^2 - q^2 + k_0^2 \frac{\Delta\kappa}{\cosh^2(x/x_0)} \right] \psi = 0 \tag{10b}$$

where q is the separation constant. The substitutions

$$\xi = \tanh(x/x_0) \tag{11a}$$

$$\psi = (1-\xi^2)^{B/2} W(\xi) \tag{11b}$$

$$b_0(b_0+1) = k_0^2 x_0^2 \Delta\kappa \tag{12a}$$

$$B^2 = (q^2 - \gamma^2 - k_0^2\kappa_S)x_0^2 \tag{12b}$$

in (10b) result in

$$(1-\xi^2)W'' - (2\lambda+1)\xi W' + \alpha(\alpha+2\lambda)W = 0 \tag{13}$$

with

$$\lambda = B + \tfrac{1}{2} \tag{14a}$$

$$\alpha = b_0 - \lambda + \tfrac{1}{2}. \tag{14b}$$

Several solutions exist for (13). When α is an integer $l = 0, 1, 2, \cdots$, we have polynomial solutions, which are the ultraspherical or Gegenbauer polynomials $C_l^{\lambda}(\xi)$. Physically, they give rise to an infinite number of discrete modes, of which some may be trapped. The radiation modes would be described by other solutions that satisfy (13) for arbitrary α (see [9]).

We will now examine the polynomial solutions $W(\xi) = C_l^{\lambda}(\xi)$ in detail. For α an integer l

$$\lambda = b_0 - l + \tfrac{1}{2} \tag{15a}$$

$$B_l = b_0 - l, \qquad l = 0, 1, 2, \cdots. \tag{15b}$$

The $C_l^{\lambda}(\xi)$ are defined by

$$C_0^{\lambda}(\xi) = 1 \tag{16a}$$

$$C_1^{\lambda}(\xi) = 2\lambda\xi \tag{16b}$$

$$(l+1)C_{l+1}^{\lambda}(\xi) = 2(l+\lambda)\xi C_l^{\lambda}(\xi) - (l+2\lambda-1)C_{l-1}^{\lambda}(\xi). \tag{16c}$$

Using (11a) and (11b) we obtain the expression for the modes

$$\psi_l(x) = [\cosh(x/x_0)]^{l-b_0} C_l^{b_0-l+\frac{1}{2}}(\tanh[x/x_0]) \tag{17}$$

where, from (12a)

$$b_0 = -\tfrac{1}{2} + \left(\tfrac{1}{4} + k_0^2 x_0^2 \Delta\kappa\right)^{1/2}. \tag{18}$$

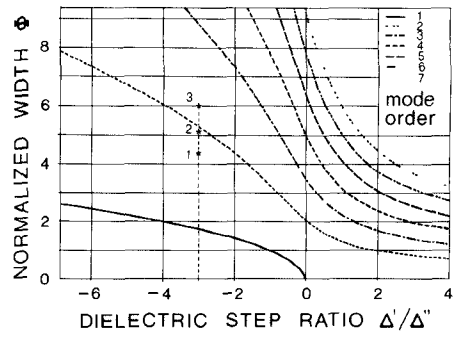

Fig. 4. Confinement curves (Φ versus Δ'/Δ'') for several mode orders.

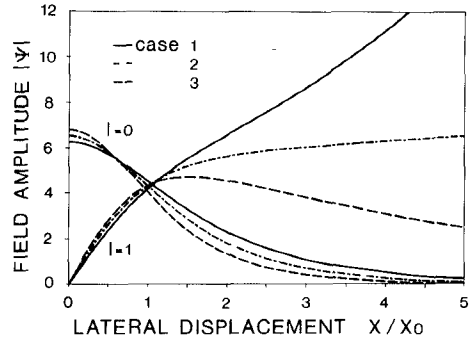

Fig. 5. Field amplitude versus lateral displacement for modes of order 0 and 1 for the 3 cases shown in Fig. 4. The curves for $l = 1$ are magnified five times.

For $x \gg x_0$, (17) becomes

$$\psi_l(x) \simeq 1/2 \exp[-(x/x_0)(b_0 - l)] \cdot C_l^{b_0-l+1/2}(1). \tag{19}$$

So to satisfy the boundary conditions, we require

$$\mathrm{Re}\{b_0 - l\} > 0. \tag{20}$$

For a given b_0, if $\mathrm{Re}\{b_0\} > 0$ there exists at least one mode that decreases as $x \to \pm\infty$, for $l = 0$ (the fundamental mode). Modes of order l such that $\mathrm{Re}\{b_0 - l\} < 0$ are still solutions of (10b) but diverge as $|x| \to \infty$, and will be designated as "leaky". Notice that, if $\mathrm{Re}\{b_0\} < 0$, even the fundamental mode becomes leaky. Condition (20) can be expressed in terms of the real and imaginary parts of $\Delta\kappa$ defining the quantities

$$\delta = \Delta'/\Delta'' \tag{21a}$$

$$\Phi = 2k_0 x_0 (\Delta'')^{1/2} \tag{21b}$$

where $\Delta\kappa = \Delta' + i\Delta''$. We obtain

$$\delta \geq \frac{(2l+1)^2 l(l+1) - \Phi^4}{\Phi^2(2l+1)^2} \tag{22}$$

as the region for lateral confinement. Fig. 4 shows Φ as a function of δ for several values of l. Fig. 5 shows the behavior of the $|\psi_l|$ for sets of parameters resulting in the (δ, Φ) points marked in Fig. 4. In particular, notice the behavior of $|\psi_1|$ when we go from "1" to "2" to "3".

The $\psi_l(x)$ will diverge for $l > l_{\max}$, where

$$l_{\max} = INT[\mathrm{Re}\{b_0\}]. \tag{23}$$

Leaky modes ($l > l_{\max}$) cannot be used when expressing a general confined field as a superposition of modes. This results in a finite discrete eigenvalue spectrum, and the need arises for a continuum in order to have a complete orthogonal set of functions. We will seek an approximate solution neglecting the continuum. For the trapped modes, the product solutions will be of the form

$$\psi_l(x)\cos(q_l y) \tag{24}$$

and the general solution will be approximated by

$$\Psi_b(x, y) \cong \sum_{l=0,2,\cdots,}^{\bar{l}_{\max}} A_l \psi_l(x)\cos(q_l y) \tag{25}$$

for a field even in x, where $\bar{l}_{\max}$ is the maximum even value of l for which ψ_l is confined. The trapped modes satisfy the orthogonality relation

$$\frac{1}{x_0}\int_{-\infty}^{\infty} \psi_l(x)\psi_l'(x)\,dx = N_l \delta_{l,l'}. \tag{26}$$

The first few normalization constants are

$$N_0 = \frac{\sqrt{\pi}\,\Gamma(b_0)}{\Gamma\left(b_0+\frac{1}{2}\right)} \tag{27a}$$

$$N_1 = \frac{2\left(b_0-\frac{1}{2}\right)^{1/2}}{(b_0-1)}\sqrt{\pi}\,\frac{\Gamma(b_0)}{\Gamma\left(b_0+\frac{1}{2}\right)} \tag{27b}$$

$$N_2 = \frac{2\sqrt{\pi}\,(b_0-3/2)^2\left(b_0-\frac{1}{2}\right)\Gamma(b_0)}{(b_0-2)\Gamma\left(b_0+\frac{1}{2}\right)} \tag{27c}$$

where $\Gamma(z)$ is the factorial function. An analytic but lengthy expression for the N_l exists but is not given here.

Solution of (8) for the confining layers proceeds as in [1]. Separation of variables is applied to (8); the lateral solution is of the form $\cos(\chi x)$ whereas the vertical solution is a decreasing exponential. Superposition is then applied; this results in an integral since no boundary conditions are available that would result in a discrete spectrum. The general solution will be

$$\Psi_a(x, y) = \int_0^{\infty} B(\chi)\cos(\chi x) \cdot \exp\left[\left(\chi^2-\gamma^2-k_a^2\right)^{1/2}(d/2-y)\right] d\chi \tag{28}$$

where

$$k_a^2 = k_0^2\kappa_A.$$

Now, (25) and (28) and their normal derivatives have to be matched at $y = \pm d/2$, the boundaries of the active layer. Matching ψ_a and ψ_b results in an expression for $B(\chi)$

$$B(\chi) = \frac{2}{\pi}\sum_{l=0,2,\cdots,}^{\bar{l}_{\max}} A_l\sqrt{N_l}\cos\left(q_l\frac{d}{2}\right)\bar{\psi}_l(\chi) \tag{29a}$$

where

$$\bar{\psi}_l(\chi) = \int_0^{\infty}\frac{\psi_l(x)}{\sqrt{N_l}}\cos(\chi x)\,dx. \tag{29b}$$

Matching the derivatives respect to y at $y = d/2$ and applying the orthogonality relation (26) yields, after using (29a)

$$\frac{4}{\pi x_0}\sum_{l=0,2,\cdots,}^{\bar{l}_{\max}} A_l\sqrt{N_l}\cos\left(ql\frac{d}{2}\right)I_{l,l'}(\gamma) = A_{l'}q_{l'}\sin\left(q_{l'}\frac{d}{2}\right)\sqrt{N_{l'}} \tag{30}$$

with $l, l' = 0, 2, \cdots, \bar{l}_{\max}$ and

$$I_{l,l'}(\gamma) = \int_0^{\infty}\bar{\psi}_l(\chi)\bar{\psi}_{l'}(\chi)\left(\chi^2-\gamma^2-k_a^2\right)^{1/2}d\chi \tag{31}$$

$$\bar{\psi}_l(\chi) = \frac{1}{\sqrt{N_l}}\sum_{m=0}^{l/2} 2^{(l-2m)}\frac{(-1)^m\Gamma\left(b_0+\frac{1}{2}-m\right)}{\Gamma\left(b_0-l+\frac{1}{2}\right)m!(l-2m)!} \cdot \sum_{k=0}^{\frac{l}{2}-m}\left\{\frac{(-1)^k\left(\frac{l}{2}-m\right)!}{\left(\frac{l}{2}-m-k\right)!k!}\cdot t(\chi, b_0+2k-l, x_0)\right\} \quad (l \text{ even}) \tag{32}$$

where

$$t(\chi, \lambda, x_0) = \frac{2^{\lambda-2}x_0}{\Gamma(\lambda)}\Gamma\left(\lambda+i\frac{\chi x_0}{2}\right)\Gamma\left(\lambda-i\frac{\chi x_0}{2}\right). \tag{33}$$

This is a finite system of linear homogeneous equations of the form

$$(\Omega^T - I)\bar{A} = 0 \tag{34}$$

where $\bar{A}^T = (A_0, A_2, \cdots, A_{\bar{l}_{\max}})$, I is the unit matrix, and the matrix elements of Ω are given by

$$\Omega_{ll'}(\gamma) = \frac{4\cos(q_l d/2)\sqrt{N_l}}{\pi x_0 q_{l'}\sin\left(q_{l'}\frac{d}{2}\right)\sqrt{N_{l'}}}I_{ll'}(\gamma). \tag{35}$$

The q_l satisfy, from (12a) and (12b)

$$q_l^2 = \gamma^2 + k_0^2\kappa_S + \frac{(b_0-l)^2}{x_0^2}. \tag{36}$$

The system of equations (34) has a nontrivial solution only if $\det(\Omega - I) = 0$. Numerical computation of the roots yields the possible values of the propagation constant γ.

IV. Numerical Results

The method was applied to a structure described by the following parameters:

$$n_A = 3.38 \qquad g_0 = 200\ \text{cm}^{-1}$$
$$\alpha_A = 50\ \text{cm}^{-1} \qquad n_0 = 3.595$$
$$\alpha_S = 50\ \text{cm}^{-1} \qquad x_0 = 6\ \mu\text{m}.$$

Direct solution of (34) involves computation of the $\Omega_{ll'}$. In general, $\Omega_{ll'} \neq \Omega_{l'l}$, but $I_{ll'} = I_{l'l}$.

Values of the modal loss = Re$\{\gamma\}$ were computed first by evaluating $I_{ll'}(\gamma)$ using the exact expression (31). This required one computation of this integral for every value of

γ, i.e., every iteration in the solution of (34). This resulted in unacceptably high computation times, in part because $\bar{\psi}_l$ involves repeated use of a gamma-function routine and also because the integrand is an oscillating function of χ. In order to improve speed, instead of solving the complete system (34) we start with a 1×1 matrix, go on to a 2×2 matrix, etc., and observe the convergence of the result. Fig. 6 shows $\mathrm{Re}\{\gamma\}$ versus Δn for 1×1 and 2×2 matrices. We see that the result converges relatively fast, so a 2×2 matrix is sufficient for our approximation. This holds for the case $\bar{l}_{\max} \geqslant 2$. For $\bar{l}_{\max} = 0$, we are limited to the 1×1 case. In Fig. 6, for $\Delta n < \sim -0.01$, $\bar{l}_{\max} = 0$. For $\Delta n > -0.01$, $\bar{l}_{\max}$ increases as shown in the figure.

In spite of this, even for $\bar{l}_{\max} = 0$, the computation time is impractically high. An increase in speed is achieved recognizing that (31) can be written as

$$I_{ll'}(\gamma) = \left(-\gamma^2 - k_a^2\right)^{1/2} \int_{-\infty}^{\infty} \left[1 + \frac{\chi^2}{-\gamma^2 - k_a^2}\right]^{1/2} \cdot \bar{\psi}_l(\chi)\bar{\psi}_{l'}(\chi)\, d\chi. \quad (37)$$

For common values of k_a^2 and γ, $|\chi^2/(-\gamma^2 - k_a^2)| \ll 1$ in the range of values of χ for which $\bar{\psi}_l(\chi)$ and $\bar{\psi}_{l'}$ are appreciably different from zero. This allows us to expand the radical in (37) using the binomial theorem and retaining only a finite number of terms. This results in

$$I_{ll'}(\gamma) = \left(-\gamma^2 - k_a^2\right)^{1/2} \left\{ \int_{-\infty}^{\infty} \bar{\psi}_l \bar{\psi}_{l'}\, d\chi + \frac{1}{2\left(-\gamma^2 - k_a^2\right)} \cdot \int_{-\infty}^{\infty} \chi^2 \bar{\psi}_l \bar{\psi}_{l'}\, d\chi - \frac{1}{8\left(-\gamma^2 - k_a^2\right)^2} \cdot \int_{-\infty}^{\infty} \chi^4 \bar{\psi}_l \bar{\psi}_{l'}\, d\chi + \cdots \right\}. \quad (38)$$

The integrals do not depend on γ, so they need to be computed only once for a given set of material parameters, and not for every value of γ, as (31) would require. Furthermore, the properties of the Fourier transform guarantee that

$$\int_{-\infty}^{\infty} \bar{\psi}_l \bar{\psi}_{l'}\, d\chi = \delta_{ll'}. \quad (39)$$

Agreement with exact computation of (31) is excellent with the first three terms in the expansion (38) and the computation time is reduced substantially, by nearly two orders of magnitude. This allows us to perform more extensive modeling using this method.

Fig. 7 shows plots of the modal loss $= \mathrm{Re}\{\gamma\}$ as a function of Δn, with g_0, the gain under the stripe, as a parameter. We notice that for each value of g_0, Δn can be decreased up to a certain value beyond which the fundamental mode becomes leaky, i.e., the antiguiding effect of the (negative) Δn offsets the guiding effect of the gain distribution.

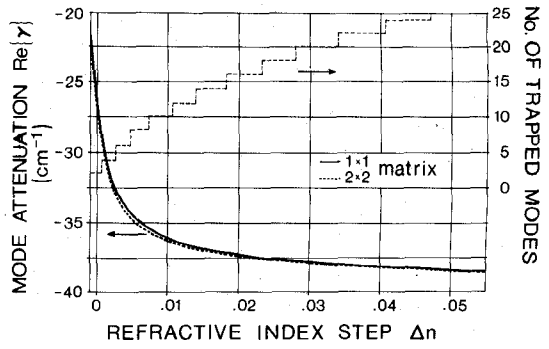

Fig. 6. Mode attenuation $\mathrm{Re}\{\gamma\}$ and number of discrete trapped modes versus Δn.

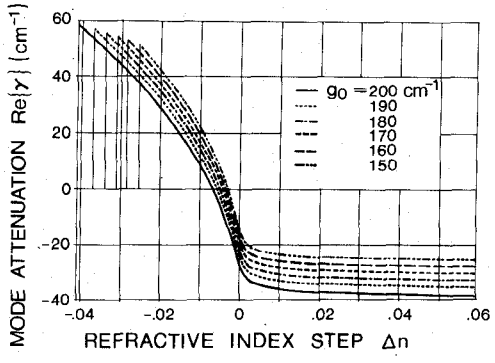

Fig. 7. Mode attenuation $\mathrm{Re}\{\gamma\}$ versus Δn for different values of g_0.

More negative values of Δn are required to offset higher values of g_0. For any given g_0, using (5), (18), and (20) with $l = 0$, it can be shown that the boundary value of Δn is

$$\Delta n = -\tfrac{1}{2} x_0^2 n_0 \left(g_0 + \alpha_S\right)^2. \quad (40)$$

These values are marked with vertical lines in Fig. 7. This relation shows that the guiding effect of the gain distribution does not depend on the individual values of g_0 (gain under the stripe) and $-\alpha_S$ (gain far away from the stripe), but only on their difference $g_0 - (-\alpha_S) = g_0 + \alpha_S$.

V. Effective-Index Calculation

The effective-index method consists basically in reducing a two-dimensional problem to an equivalent one-dimensional one. In our case, the two-dimensional character of the problem is given by the dependence of the dielectric constant on x and y. As a first approximation, the variation in one direction (in our case: x) is neglected; this is justified if this variation is much less than that in the y direction. This is equivalent to approximating the waveguide with a simple three-layer guide whose dielectric constants do not vary with x. The solution of this problem yields the transverse or vertical variation of the field. Next, the original equation describing the two-dimensional equation in x can be solved for the lateral variation of the field, and the overall solution is approximated by the product of this lateral field and the vertical field found from the

three-layer problem. We start with the wave equation in two dimensions, which is obtained merging (7) and (8)

$$\nabla_t^2\Psi + \left[\gamma^2 + k_0^2\kappa(x, y)\right]\Psi = 0 \tag{41}$$

where

$$\kappa(x, y) = \begin{cases} \kappa_A, & |y| \geq d/2 \\ \kappa_S + \dfrac{\Delta\kappa}{\cosh^2(x/x_0)}, & |y| < d/2 \end{cases}. \tag{42}$$

For the simple three-layer guide we assume $\kappa(x) = \kappa_0$ inside the active layer. We then have

$$\frac{d^2\phi}{dy^2} = \begin{cases} -q^2\phi & |y| \leq d/2 \quad (43a) \\ p^2\phi & |y| > d/2 \quad (43b) \end{cases}$$

with

$$p^2 + q^2 = k_0^2[\kappa_0 - \kappa_A] \tag{44a}$$

$$p = q\tan(qd/2). \tag{44b}$$

Now, we transform (41) making $\Psi(x, y) = \psi(x)\phi(y)$, multiplying it by $\phi^*(y)$, and integrating it over y from $-\infty$ to ∞, taking into account (42) and (43) and defining the confinement factor

$$\Gamma \equiv \frac{\int_{-d/2}^{d/2} \phi^*(y)\phi(y)\,dy}{\int_{-\infty}^{\infty} \phi^*(y)\phi(y)\,dy}. \tag{45}$$

We obtain

$$\frac{d^2\psi}{dx^2} + \left[\gamma^2 - q_{\text{eff}}^2 + k_0^2\kappa_{S\text{eff}} + k_0^2\frac{\Delta\kappa_{\text{eff}}}{\cosh^2(x/x_0)}\right]\psi = 0 \tag{46}$$

with

$$q_{\text{eff}}^2 = \Gamma k_0^2 x_0 - p^2 - k_0^2\kappa_A \tag{47a}$$

$$\kappa_{S\text{eff}} = \Gamma\kappa_S \tag{47b}$$

$$\Delta\kappa_{\text{eff}} = \Gamma\Delta\kappa. \tag{47c}$$

Equation (46) has the same form as (10b). It will also have polynomial solutions similar to (17) that represent trapped modes

$$\psi_l(x) = \left[\cosh(x/x_0)\right]^{l - b_{0\text{eff}}} C_l^{b_{0\text{eff}} - l + \frac{1}{2}}\left(\tanh\frac{x}{x_0}\right) \qquad l = 0, 1, 2, \cdots \tag{48}$$

where $b_{0\text{eff}}$, $\Delta\kappa_{\text{eff}}$, and $\kappa_{S\text{eff}}$ satisfy relations identical to (12b), (15b), and (18). For the fundamental mode, $l = 0$, $B = b_{0\text{eff}}$, and using (44b), we obtain

$$\gamma^2 = -k_0^2\kappa_A - \frac{b_{0\text{eff}}^2}{x_0^2} - \left(p^2 - k_0^2\Gamma\Delta\kappa\right) \tag{49}$$

for the propagation constant.

VI. Discussion

Values of γ obtained using (49) are compared with those obtained with the numerical method in Fig. 8. Solutions are very close for all values of Δn for which the mode exhibits a gain which is relatively high and with low sensitivity to Δn. The results differ most in the range of Δn for which the mode has a net loss or has a relatively low gain with higher sensitivity to Δn. This is the same region for which only one trapped mode exists, so the error in the numerical method is the greatest because the neglected continuum is more important.

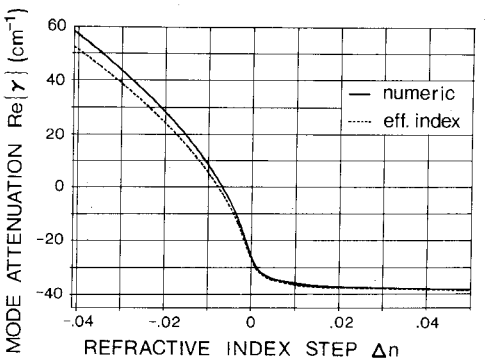

Fig. 8. Mode attenuation $\text{Re}\{\gamma\}$ versus Δn for numeric and effective-index methods, for $g_0 = 200\ \text{cm}^{-1}$.

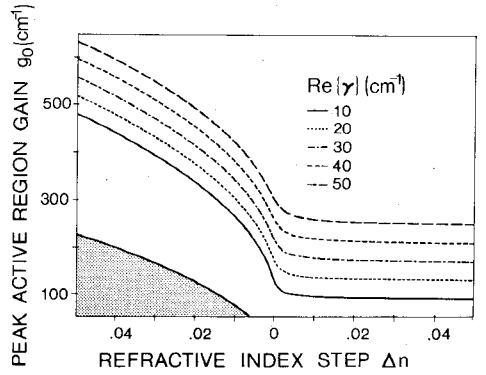

Fig. 9. Peak active region gain g_0 versus Δn for several values of $\text{Re}\{\gamma\}$. Dotted area indicates region where fundamental mode becomes leaky.

Fig. 9 gives the required value of the peak power gain g_0 under the stripe to obtain a given modal gain G, as a function of Δn, using the effective-index method. Also included is the region for which the fundamental mode becomes leaky. Figs. 10–12 show the normalized lateral field distributions for different values of Δn. The increasing antiguiding effect of decreasing Δn is apparent. The distance x at which the gain is zero (loss/gain boundary) is shown in these figures with vertical dashed lines. It can be shown to be given by

$$\bar{x} = x_0\cosh^{-1}\left(1 + \frac{g_0}{\alpha_S}\cdot\frac{n_0}{n_S}\right)^{1/2}. \tag{50}$$

For the set of parameters considered, $\bar{x} = 1.45\ x_0$. This allows us to qualitatively understand why the modes have the loss (gain) indicated. The vertical confinement factor Γ did not vary appreciably with Δn; a typical value for the case considered was $\Gamma \simeq 0.4963$. We see that lateral variations in the refractive index affect the gain much more by altering the lateral field distribution than by affecting the vertical variation.

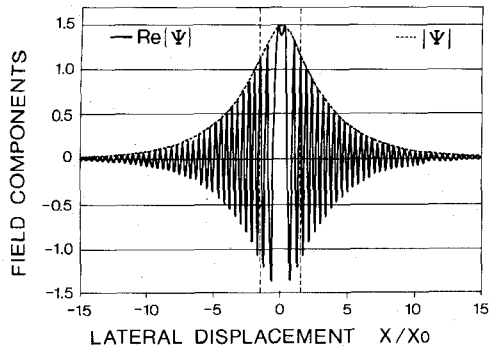

Fig. 10. Normalized lateral field distribution, for $\Delta n = -0.0156$. The resulting modal loss is 20 cm^{-1}. Vertical dashed lines indicate the distance at which the gain inside the active layer is zero.

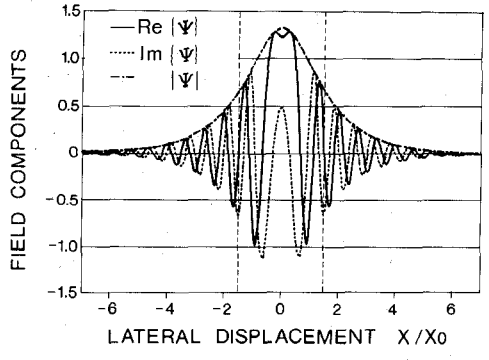

Fig. 11. Normalized lateral field distribution for $\Delta n = -0.006$. $\mathrm{Re}\{\gamma\} = -4.46$ cm^{-1} (gain). Vertical dashed lines have the same meaning as in Fig. 10.

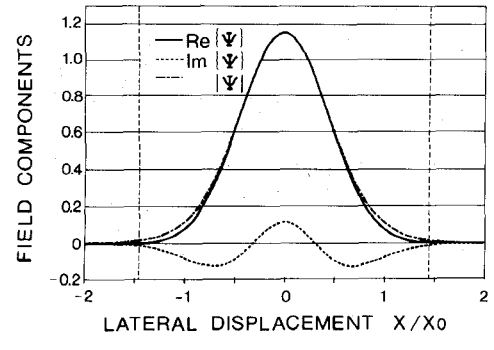

Fig. 12. Normalized lateral field distribution for $\Delta n = 0.002$. The modal gain, $-\mathrm{Re}\{\gamma\}$, is now 32.3 cm^{-1}.

The effective-index method is seen to be a fast and relatively accurate way to obtain the field distributions for the class of waveguides considered, for which the numerical method we used is not practical for extensive modeling due to its long computation time in spite of all approximations. The remarkable agreement between the effective-index method and experimental results found by other workers ([10]) increases our confidence in this powerful approximate method.

References

[1] J. K. Butler and J. B. Delaney, "A rigorous boundary value solution for the lateral modes of stripe geometry injection lasers," *IEEE J. Quantum Electron.*, vol. QE-14, pp. 507–513, July 1978.

[2] T. L. Paoli, "Waveguiding in a stripe-geometry junction laser," *IEEE J. Quantum Electron.*, vol. QE-13, pp. 662–668, Aug. 1977.

[3] W. Streifer, D. Scifres, and R. Burnham, "Analysis of gain-induced waveguiding in stripe-geometry injection lasers," *IEEE J. Quantum Electron.*, vol. QE-14, pp. 418–427, June 1978.

[4] P. M. Asbeck, D. A. Cammack, and J. J. Daniele, "Non-gaussian fundamental mode patterns in narrow-stripe-geometry lasers," *Appl. Phys. Lett.*, vol. 33, pp. 504–506, Sept. 1978.

[5] R. M. Knox and P. P. Toulios, "Integrated circuits for the millimeter through optical frequency range," in *Proc. MRI Symp. Submillimeter Waves*, J. Fox, Ed. New York: Brooklyn Polytechnic, 1970.

[6] W. Streifer and E. Kapon, "Application of the equivalent-index method to DH diode lasers," *Appl. Opt.*, vol. 18, pp. 3724–3725, Nov. 1979.

[7] J. Buus, "A model for the static properties of DH lasers," *IEEE J. Quantum Electron.*, vol. QE-15, pp. 734–739, Aug. 1979.

[8] J. K. Butler and J. B. Delaney, "Field solutions for the lateral modes of stripe geometry injection lasers," *IEEE J. Quantum Electron.*, vol. QE-16, pp. 1326–1328, Dec. 1980.

[9] A. Erdelyi, W. Magnus, F. Oberhettinger, and F. Tricomi, "Higher transcendental functions," vol. I—Bateman Manuscript Project. New York: McGraw-Hill, 1953, Sect. 3.15, 3.16.

[10] J. K. Butler and D. Botez, "Mode characteristics of non-planar double-heterojunction and large-optical cavity laser structures," *IEEE J. Quantum Electron.*, vol. QE-18, pp. 952–961, June 1982.

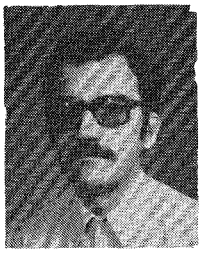

Alfredo Linz was born in 1951 in Quito, Ecuador. He received the degree of Ingeniero en Electronica y Telecommunicaciones from Escuela Politecnica Nacional, Quito, in 1977, summa cum laude. From 1977 to 1979 he served as Instructor at EPN. Through the Fulbright Program he was awarded as assistantship at Southern Methodist University, Dallas, TX, where he obtained the M.S.E.E. degree in 1981, and is currently working toward a Ph.D. degree.

Mr. Linz's interests include optical communication, quantum electronics, and digital systems. He is a member of Tau Beta Pi.

Jerome K. Butler (S'59–M'65–SM'78) received the B.S. degree from Louisiana Polytechnic University, Ruston, in 1960, and the M.S. and Ph.D. degrees from the University of Kansas, Lawrence, in 1962, and 1965, respectively.

From 1960 to 1965 he was a Research Assistant at the Center for Research in Engineering Sciences, University of Kansas, Lawrence. His research was related to electromagnetic-wave propagation and to the optimization and synthesis techniques of antenna arrays. In 1965 he joined the staff of the School of Engineering and Applied Science, Southern Methodist University, Dallas, TX, where he is now Professor of Electrical Engineering. His primary research areas are solid-state injection lasers, radiation and detection studies of lasers, communication and imaging systems, integrated optics and the application of integrated optical circuits, and quantum electronics. In the summer from 1969 to 1982 he was a member of the Technical Staff, RCA Laboratories, Princeton, NJ, where he did research concerned with electromagnetic-wave propagation in solid-state injection lasers. Dr. Butler is coauthor of the book *Semiconductor Lasers and Heterojunction LED's* (New York: Academic). He has held consulting appointments with the Central Research Laboratory, Texas Instruments, Inc., the Geotechnical Corporation of Teledyne, Inc., Earl Cullum Associates, Dallas, TX, and the University of California Los Alamos Scientific Laboratory.

Dr. Butler is a member of Sigma Xi, Tau Beta Pi, Eta Kappa Nu, and is a Registered Professional Engineer in the State of Texas.